Supporting Information

Controllable Synthesis of Ultrathin Layered Transition Metallic Hydroxide /Zeolitic Imidazolate Framework-67 Hybrid Nanosheets for High-Performance Supercapacitors

Chunli Liu[a], Yang Bai[a,b]*, Ji Wang[a], Ziming Qiu[a], Huan Pang[a]*

[a] School of Chemistry and Chemical Engineering, Yangzhou University, Yangzhou, 225000, Jiangsu, P. R. China.
[b] State Key Laboratory of Coordination Chemistry, Nanjing University, China.
E-mail:
huanpangchem@hotmail.com, panghuan@yzu.edu.cn (H. Pang),
ybai@yzu.edu.cn (Y. Bai)

Contents

1 Experimental

1.1Materials

Cobalt nitrate hexahydrate ($Co(NO_3)_2·6H_2O$), cobalt chloride hexahydrate ($CoCl_2·6H_2O$), manganese nitrate tetrahydrate ($Mn(NO_3)_2·4H_2O$), nickel nitrate dihydrate ($Ni(NO_3)_2·2H_2O$), zinc nitrate hexahydrate ($Zn(NO_3)_2·6H_2O$), 2-MeIm, and *N,N*-dimethylformamide (DMF) were bought from Aladdin Industrial Corporation.

1.2 Preparation of ultrathin *α*-Co(OH)₂/ZIF-67 nanosheets

The 2D α-$Co(OH)_2$/ZIF-67 nanosheets can be obtained by a one-pot co-precipitation reaction. $Co(NO_3)_2·6H_2O$ (1 mmol) was dissolved in a mixture solution including 15 mL of DMF and 15 mL of H_2O (denoted by solution A) and 2-MeIm (4 mmol) was dissolved in the solution with the same composition (denoted by solution B). After stirring for 15 min, the solution A was injected into the solution B at once and the mixture was stirred at room temperature for 24 h. Finally, the sample was centrifuged and washed with distilled H_2O and ethanol to remove residue followed by freeze-drying.

1.3 Preparation of ultrathin *α*-$CoM_{0.05}(OH)_x$/ZIF-67 nanosheets

The 2D α-$CoM_{0.05}(OH)_x$/ZIF-67 nanosheets can be obtained by using the similar method as α-$Co(OH)_2$/ZIF-67. One mmol $Co(NO_3)_2·6H_2O$ and 0.05 mmol $M(NO_3)_2$ were dissolved in a mixture solution including 15 mL of DMF and 15 mL of H_2O (denoted by solution A) and 4 mmol 2-MeIm was dissolved in the solution with the same composition (denoted by solution B). After stirring for 15 min, the solution A was injected into the solution B at once and the mixture was stirred at room temperature for 24 h. Finally, the sample was centrifuged and washed with distilled H_2O and ethanol to remove residue. The α-$CoM_{0.05}(OH)_x$/ZIF-67 was obtained after freeze-drying.

1.4 Preparation of 2D ultrathin *α*-$Co(OH)_2$ nanosheets

The 2D α-$Co(OH)_2$ nanosheets can be obtained by a plain precipitation reaction. 1 mmol $CoCl_2·6H_2O$ was dissolved in 30 mL distilled H_2O, and $NH_3·H_2O$ was added to regulate the alkaline environment. After stirring for 24h, the sample was centrifuged and washed with water and ethanol to remove residue. The α-$Co(OH)_2$ was obtained after freeze-drying.

1.5 Preparation of 2D β-$Co(OH)_2$ nanosheets

The 2D β-$Co(OH)_2$ nanosheets can be obtained by a plain precipitation reaction. 1 mmol $Co(NO_3)_2 \cdot 6H_2O$ was dissolved in 60 mL distilled H_2O, and KOH was added to regulate the alkaline environment. After stirring for 24h, the sample was centrifuged and washed with water and ethanol to remove residue. The β-$Co(OH)_2$ was obtained after freeze-drying.

1.6 Materials Characterization

The detailed microstructures and morphology were observed by field emission scanning electron microscopy (FE-SEM, Zeiss-Supra55) under the acceleration voltage of 5.0 kV) and transmission electron microscopy (TEM, JEM-2100 instrument). High-resolution TEM (HRTEM) images, selected area electron diffraction (SAED) images, and elemental mapping were captured on a Tecnai G2 F30 at an acceleration voltage of 300 kV. The atomic force microscope (AFM) was performed into this sample using a Nanoscope V Multimode 8 scanning probe microscope from Bruker Corporation. The crystal phase of the as-synthetized products was performed by X-ray diffraction (XRD) on a Bruker D8 Advanced X-ray Diffractometer (Cu-Kα radiation: λ = 0.15406 nm). Fourier transform infrared (FTIR) spectra were supplied to characterize their information of chemical bonds or functional groups on a Cary 610/670. The specific surface area was obtained from the N_2 adsorption/desorption isotherms and was calculated by the Brunauer-Emmett-Teller (BET) method on Autosorb IQ3. The surface composition and valence states were analyzed by X-ray photoelectron spectra (XPS) on a Thermo Scientific ESCALAB 250 apparatus.

1.7 Electrochemical tests with a three-electrode system

For the three-electrode cell, the working electrode was obtained by mixing the active materials, acetylene black, and polytetrafluoroethylene (PTFE) at a weight ratio of 80 : 15 : 5. Then, a few drops of isopropanol were added into the above mixture and coated on a piece of nickel foam (1×1 cm^{-2}, current collector), which was next drying and pressed into a thin foil at a pressure of 8~10 MPa. The typical mass loading of the electrode material was 1.0~1.5 mg. The reference and counter electrode were Hg/HgO (3.0 M KOH) and Pt wire, respectively. The cyclic voltammetry (CV), galvanostatic charge discharge (GCD), and electrochemical impedance spectra (EIS) were tested on a CHI 760E electrochemical workstation in 3.0 M KOH. The specific capacitance (C) was calculated according to the following equation:

$$C = \frac{\int I\,dt}{m\,\Delta V} \quad \text{(S1)}$$

$$C = \frac{I\,\Delta t}{m\,\Delta V} \quad \text{(S2)}$$

here, I represents discharge current (A), Δt represents discharge time (s), m represents mass of electroactive components (g) and ΔV represents potential window (V).

1.8 Evaluations with a two-electrode asymmetric supercapacitor

As for the manufacture of asymmetrical supercapacitor, α-$CoMn_{0.05}(OH)_x$/ZIF-67 material and AC were used as positive electrode and negative electrode, respectively. The α-$CoMn_{0.05}(OH)_x$/ZIF-67 (or AC), acetylene black, and PTFE were milled according to the above proportions and coated on nickel foam. The electrochemical tests of CV and GCD were also tested on a CHI 760E electrochemical workstation in 3.0 M KOH. The C was calculated according to the formula (S1) and (S2), and the power density (P, W kg^{-1})/energy density (E, Wh kg^{-1}) was calculated according to the following equations:

$$E = \frac{C\,\Delta V^2}{2} \quad \text{(S3)}$$

$$P = \frac{E}{\Delta t} \quad \text{(S4)}$$

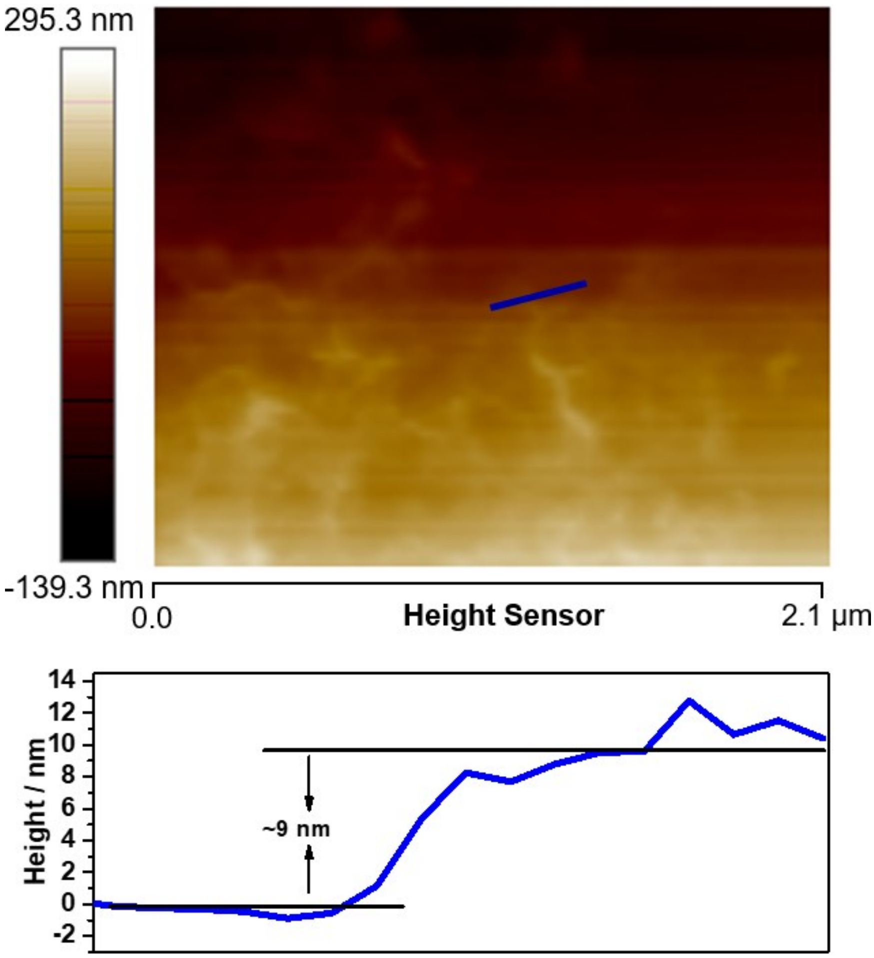

Fig. S1. AFM image and the corresponding thickness of α-$Co(OH)_2$/ZIF-67.

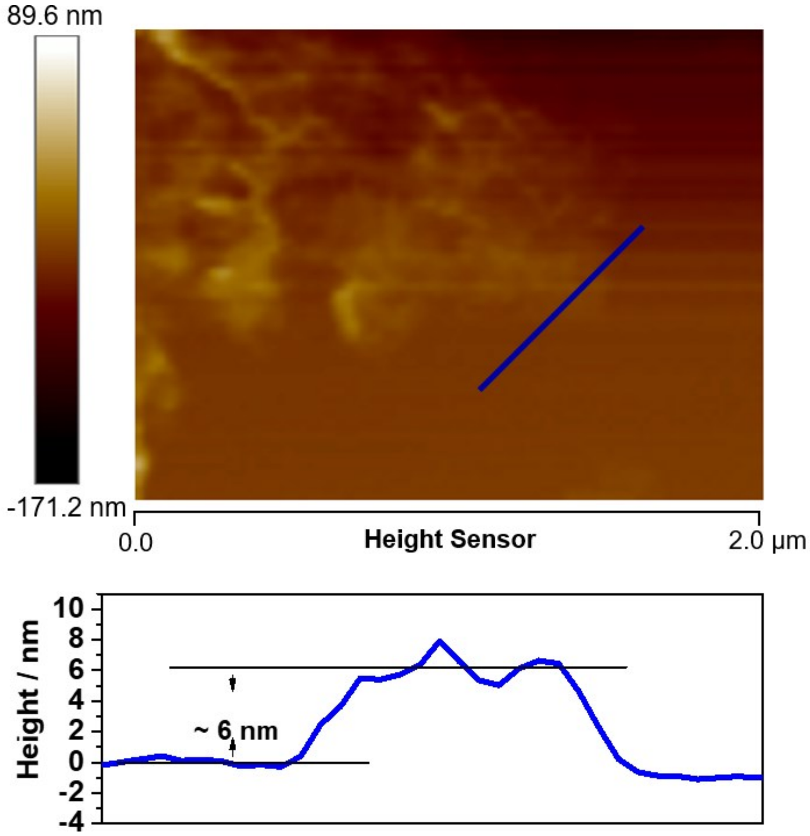

Fig. S2. AFM image and the corresponding thickness of α-$CoNi_{0.05}(OH)_x$/ZIF-67.

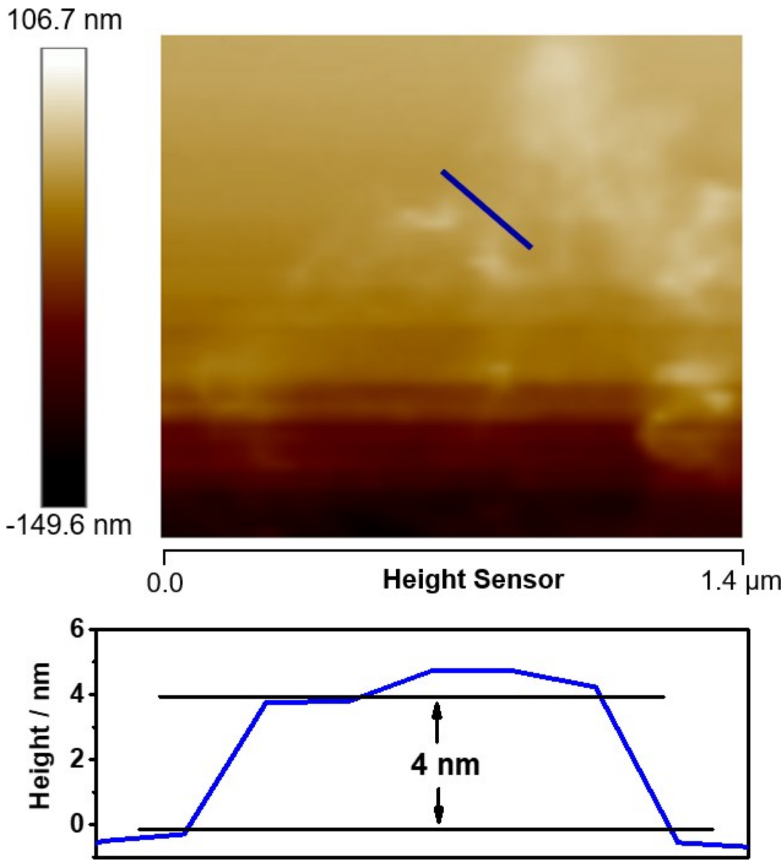

Fig. S3. (a) AFM image and the corresponding thickness of α-$CoZn_{0.05}(OH)_x$/ZIF-67.

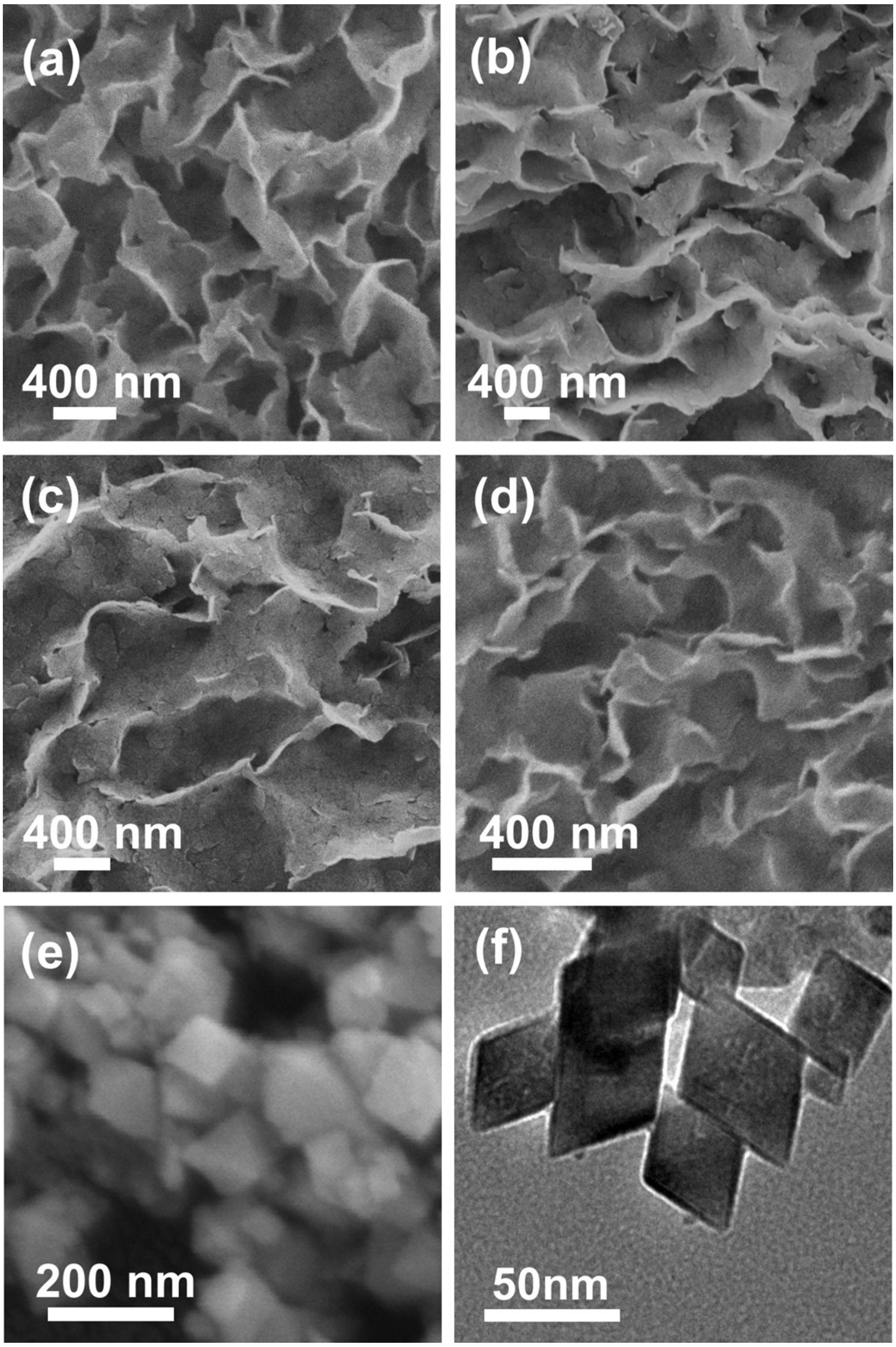

Fig. S4. (a-e) SEM and (f) TEM images of α-$CoMn_x(OH)_x$/ZIF-67 with diverse ratios of Co:Mn = (a) 1:0.01, (b) 1:0.1, (c) 1:0.5, (d) 1:1 and (e, f) 0:1.

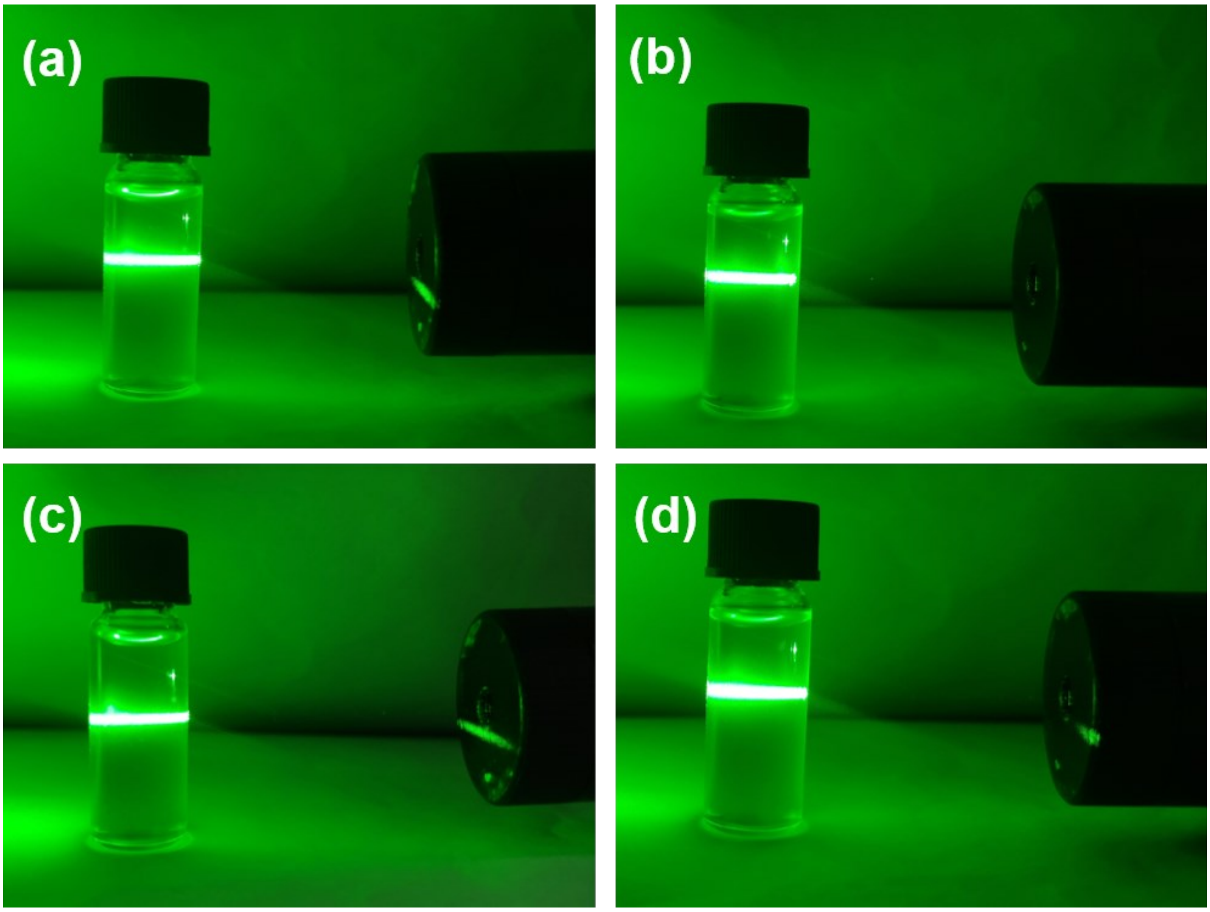

Fig. S5. The Tyndall light scattering of (a) α-$Co(OH)_2$/ZIF-67, (b) α-$CoMn_{0.05}(OH)_x$/ZIF-67, (c) α-$CoNi_{0.05}(OH)_x$/ZIF-67, (d) α-$CoZn_{0.05}(OH)_x$/ZIF-67 nanosheets in ethanol solution.

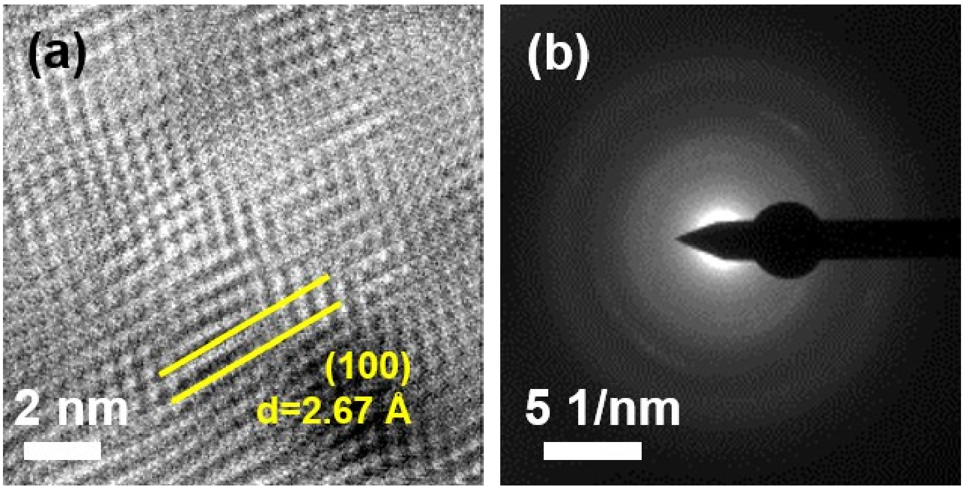

Fig. S6. (a) HRTEM and (b) SAED images of α-$CoNi_{0.05}(OH)_x$/ZIF-67.

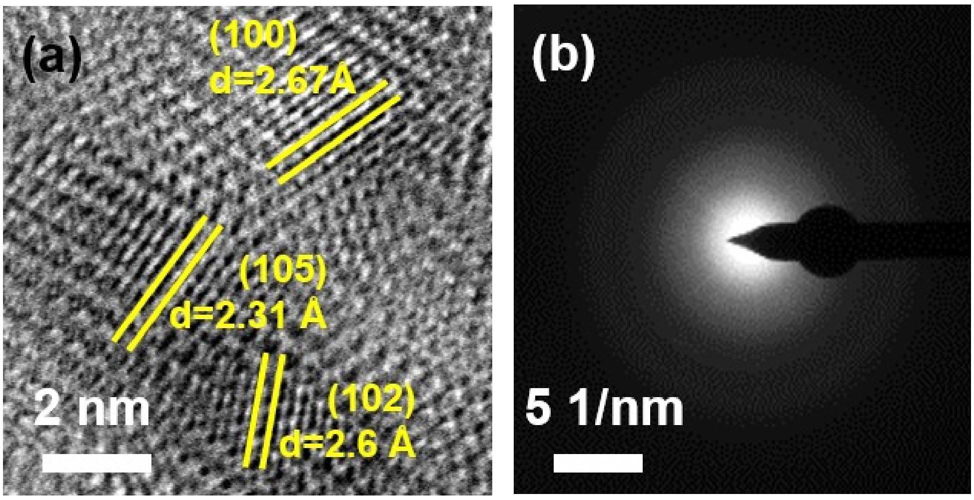

Fig. S7. (a) HRTEM and (b) SAED images of α-$CoZn_{0.05}(OH)_x$/ZIF-67.

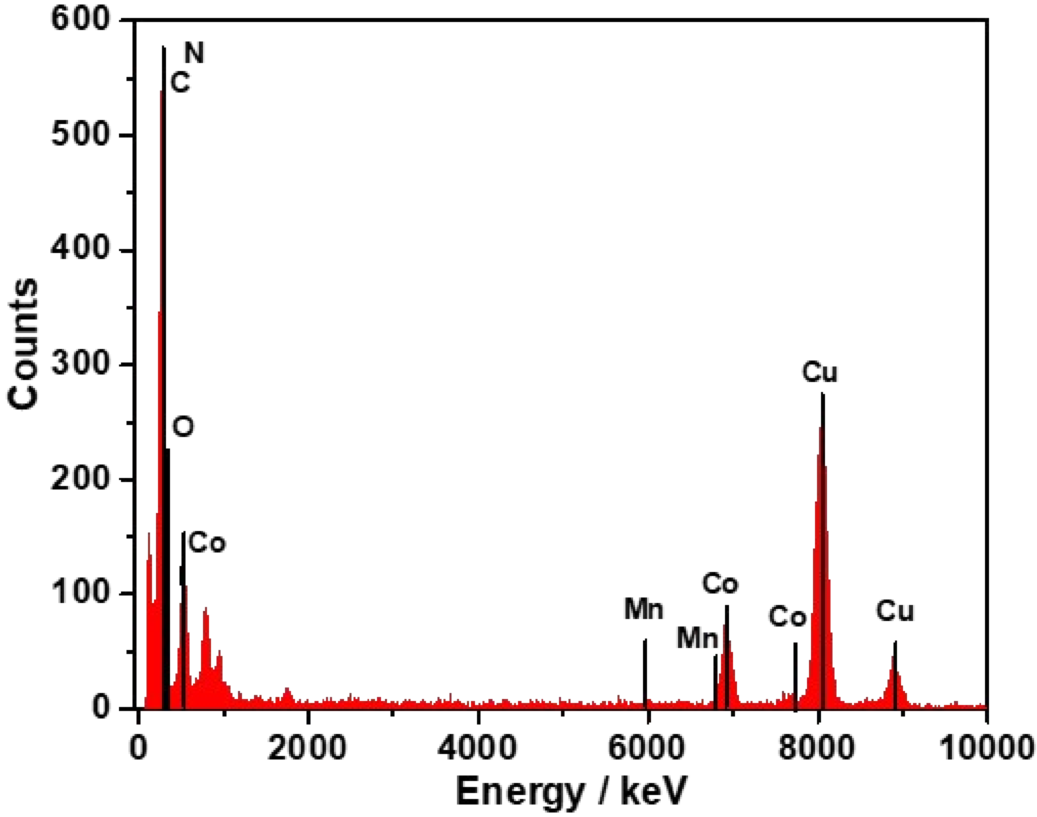

Fig. S8. EDS analysis of α-$CoMn_{0.05}(OH)_x$/ZIF-67.

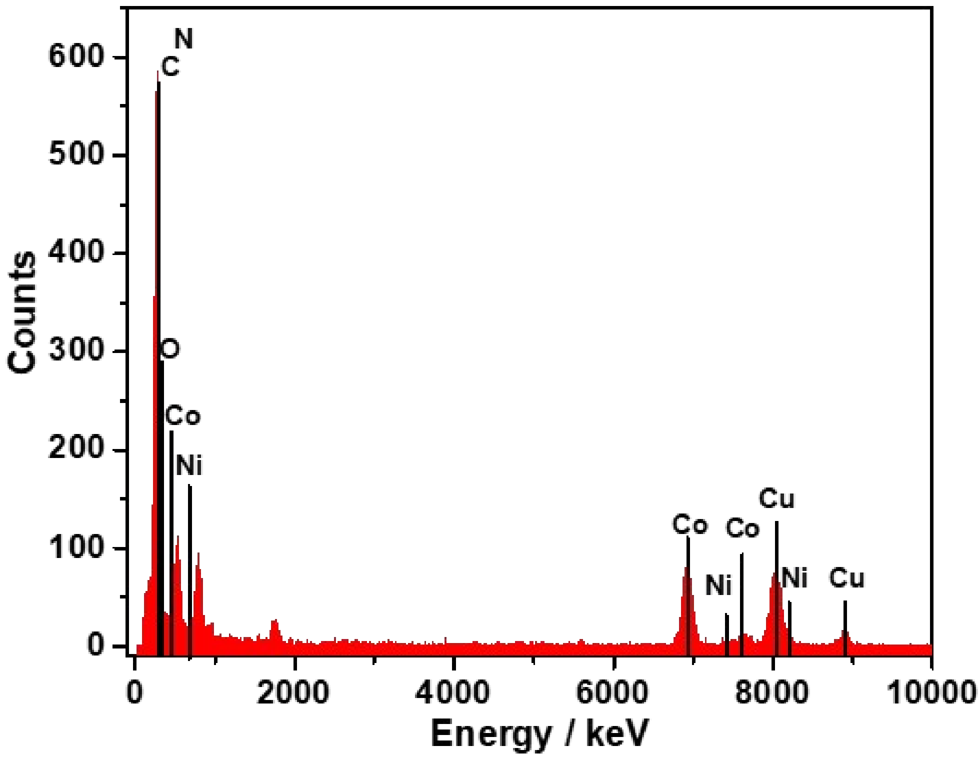

Fig. S9. EDS analysis of α-$CoNi_{0.05}(OH)_x$/ZIF-67.

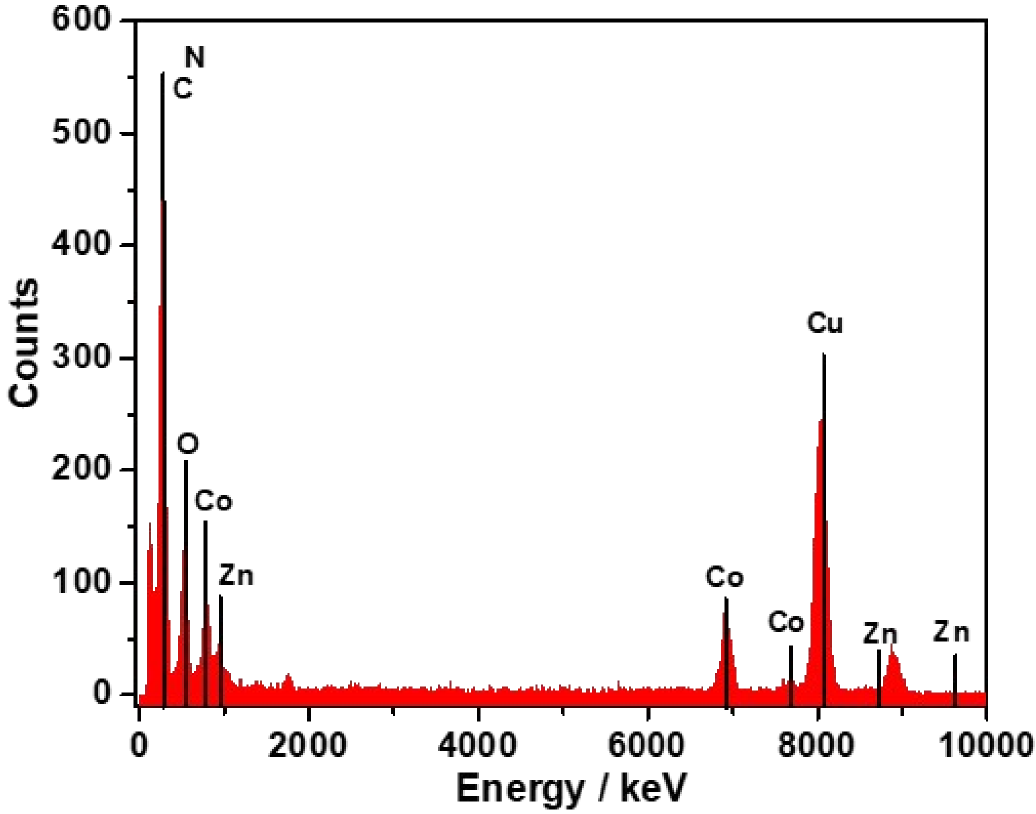

Fig. S10. EDS analysis of α-$CoZn_{0.05}(OH)_x$/ZIF-67.

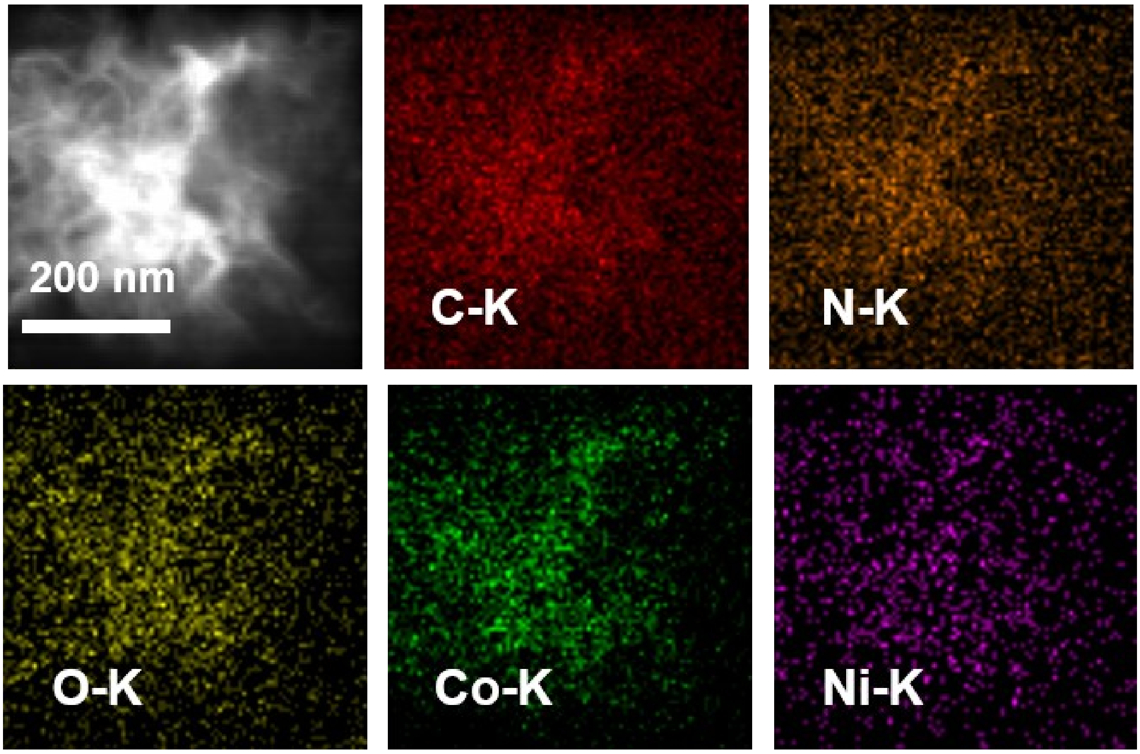

Fig. S11. Elemental mapping of C-K, N-K, O-K, Co-K and Ni-K of α-$CoNi_{0.05}(OH)_x$/ZIF-67.

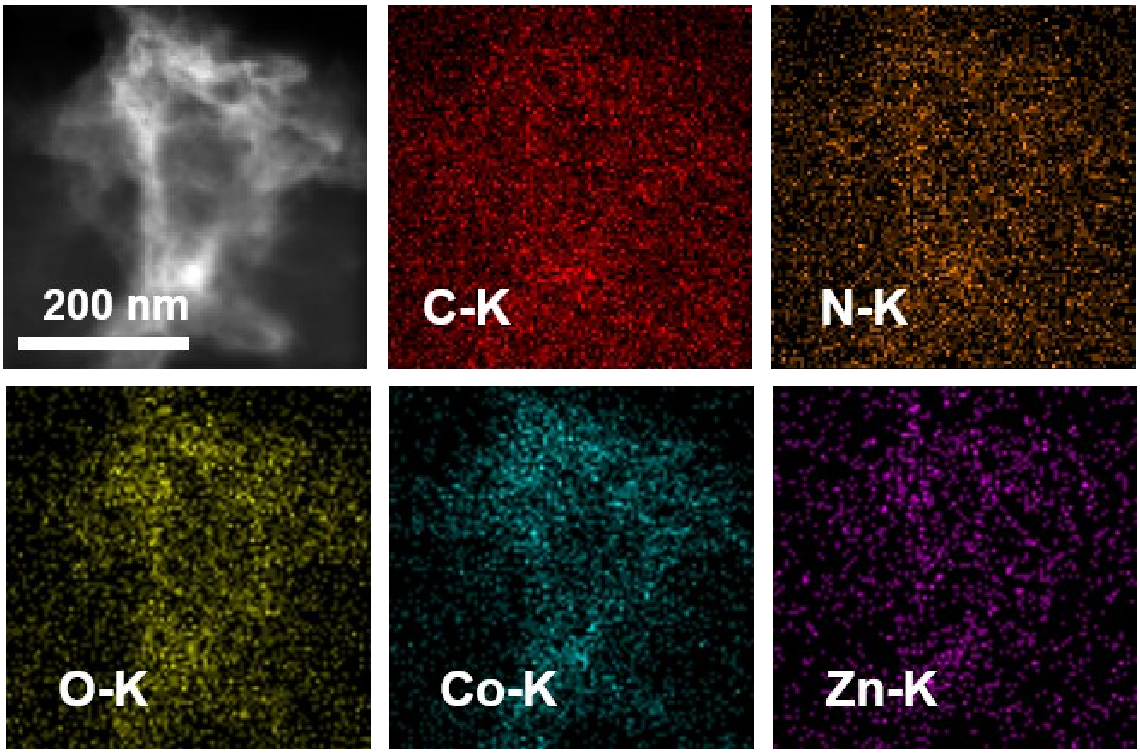

Fig. S12. Elemental mapping of C-K, N-K, O-K, Co-K and Zn-K of α-$CoZn_{0.05}(OH)_x$/ZIF-67.

Table S1. The weight % and atomic % of related elements in the α-$CoM_{0.05}(OH)_x$/ZIF-67.

	α-$CoMn_{0.05}(OH)_x$/ZIF-67		**α-$CoNi_{0.05}(OH)_x$/ZIF-67**		**α-$CoZn_{0.05}(OH)_x$/ZIF-67**	
Element	Weight %	Atomic %	Weight %	Atomic %	Weight %	Atomic %
C	82.90	90.27	81.37	89.75	80.57	88.75
N	1.45	1.36	2.58	2.44	1.58	1.49
O	8.20	6.70	6.94	5.75	9.56	7.91
Co	7.06	1.56	8.59	1.93	7.55	1.69
M	0.36	0.08	0.48	0.11	0.71	0.14

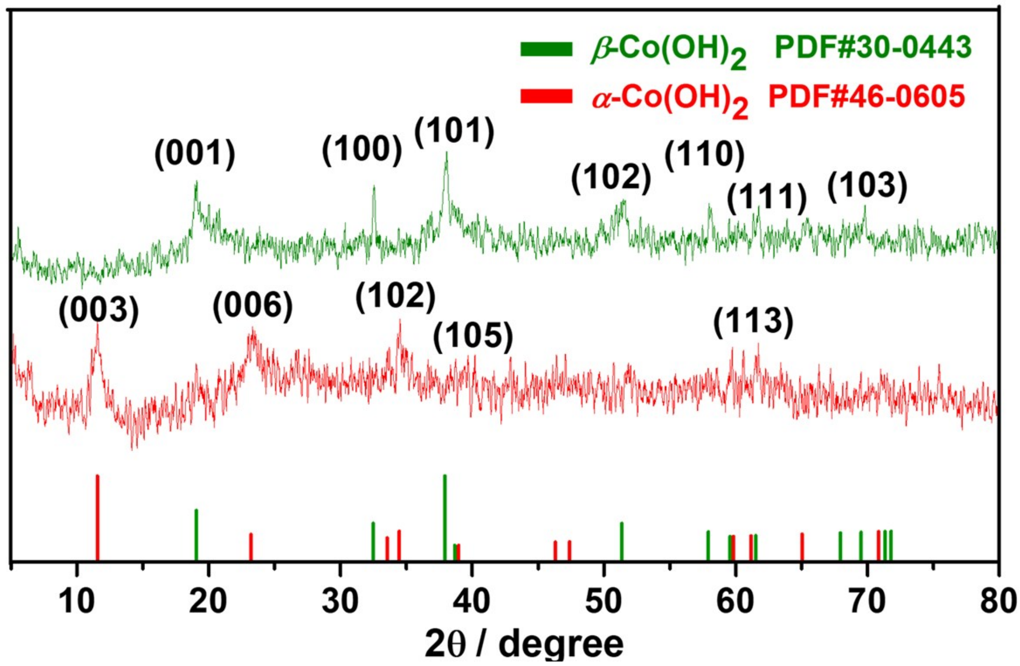

Fig. S13. XRD patterns of β-Co(OH)$_2$ and α-Co(OH)$_2$. The XRD patterns indicate two different crystalline types of the hydroxides.

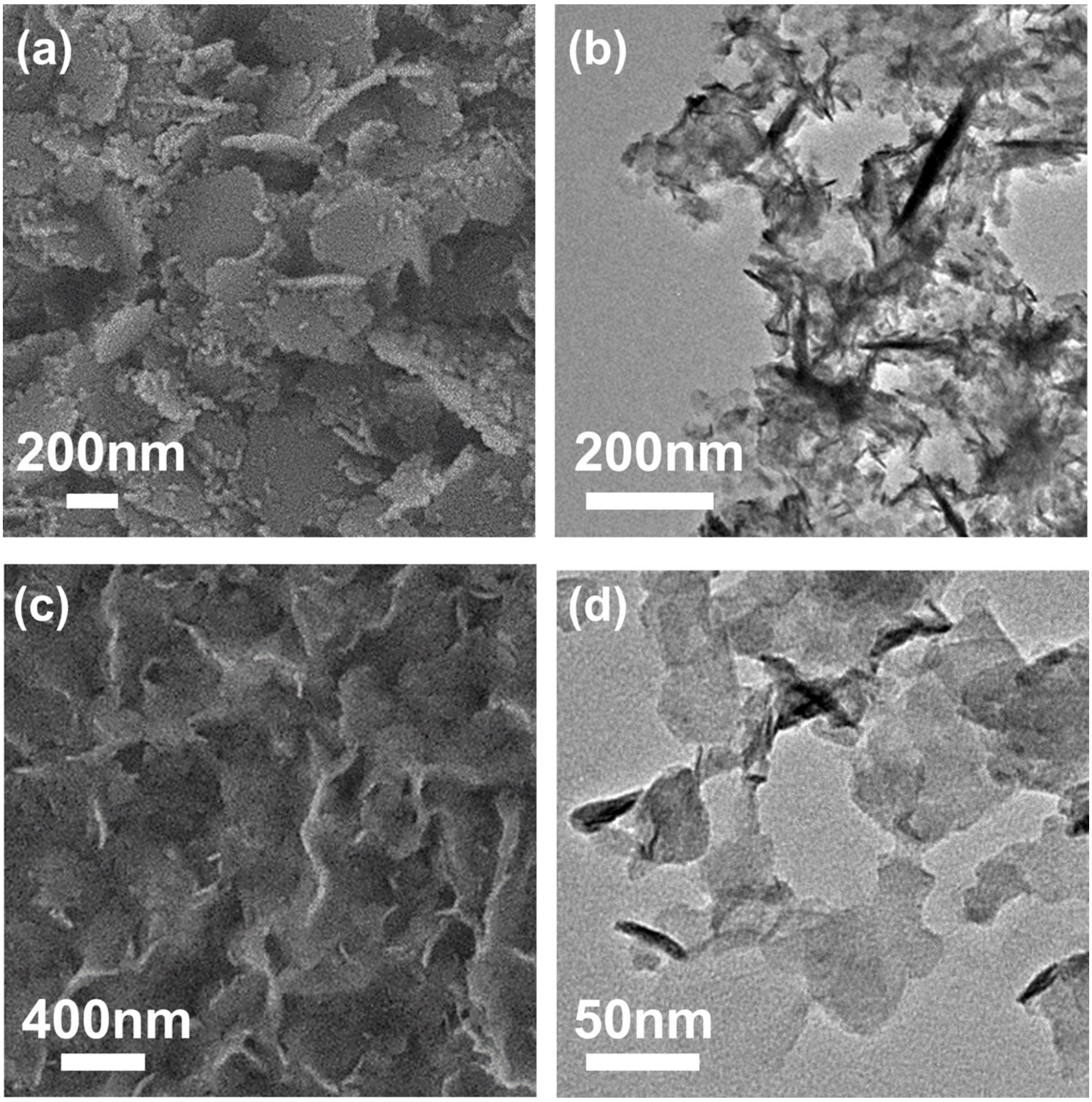

Fig. S14. SEM images of (a) β-$Co(OH)_2$ and (c) α-$Co(OH)_2$. TEM images of (b) β-$Co(OH)_2$ and (d) α-$Co(OH)_2$.

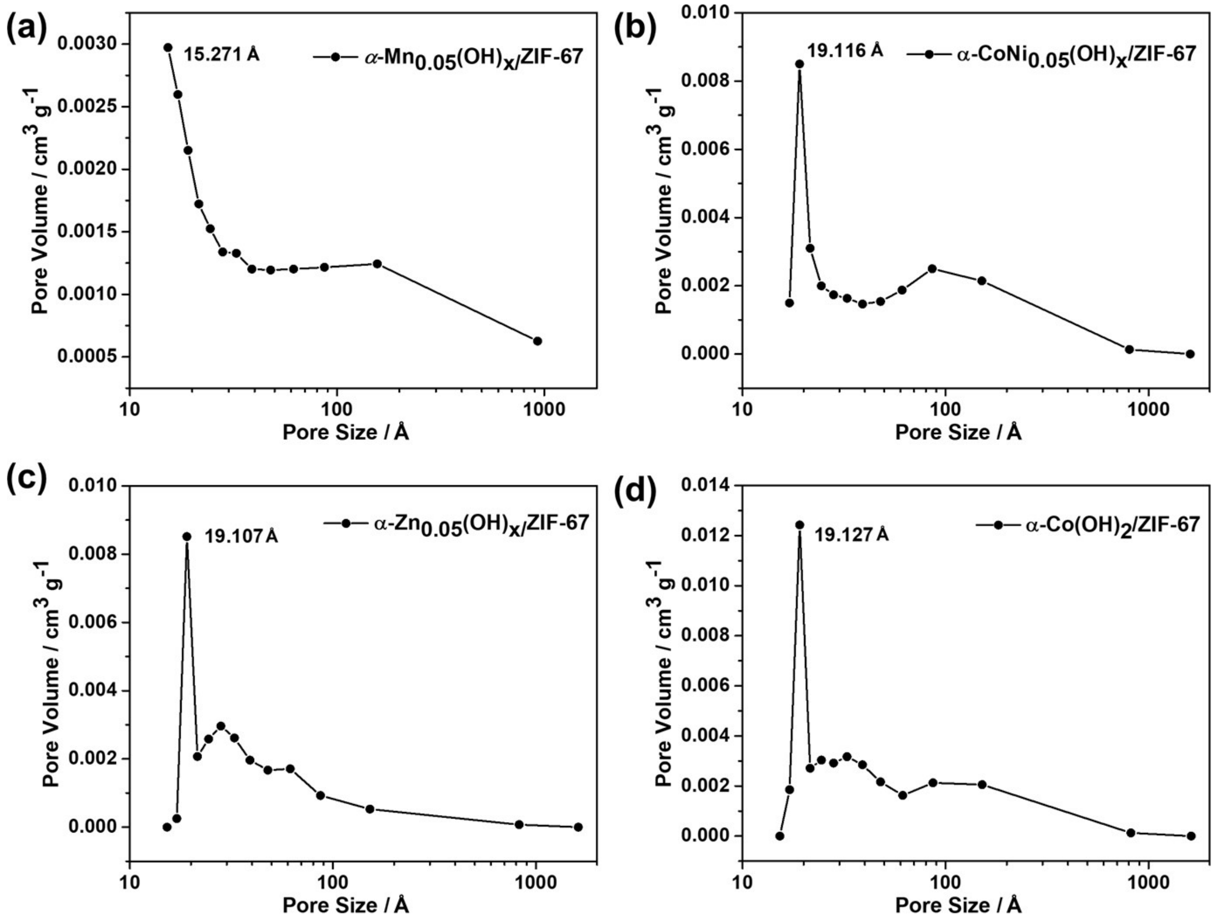

Fig. S15. The pore-size distribution of (a) α-$Co(OH)_2$/ZIF-67, (b) α-$CoMn_{0.05}(OH)_x$/ZIF-67, (c) α-$CoNi_{0.05}(OH)_x$/ZIF-67, (d) α-$CoZn_{0.05}(OH)_x$/ZIF-67.

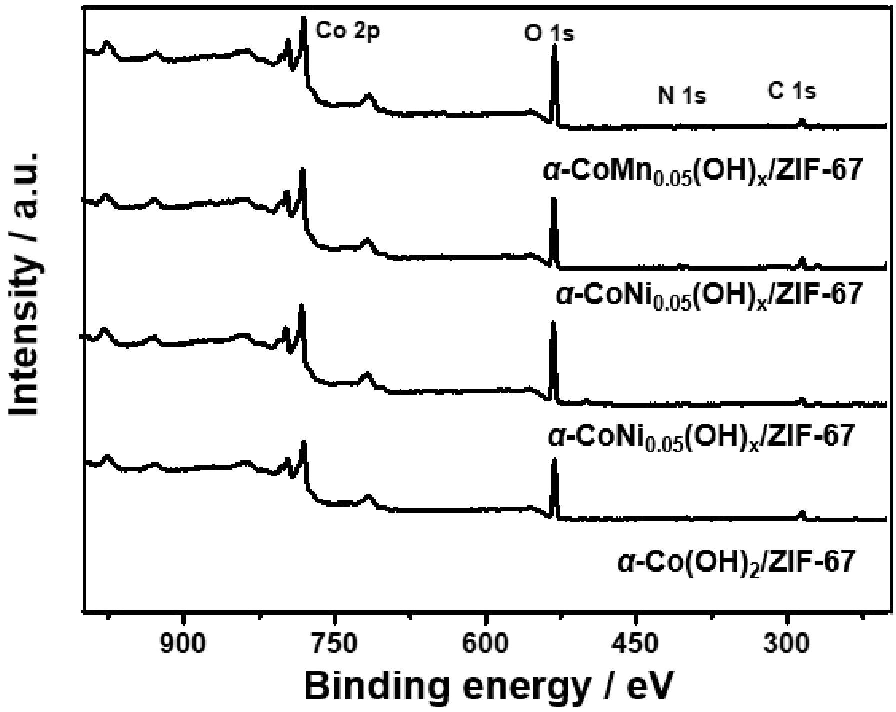

Fig. S16. Full-survey XPS spectrum of α-$Co(OH)_2$/ZIF-67 and α-$CoM_{0.05}(OH)_x$/ZIF-67.

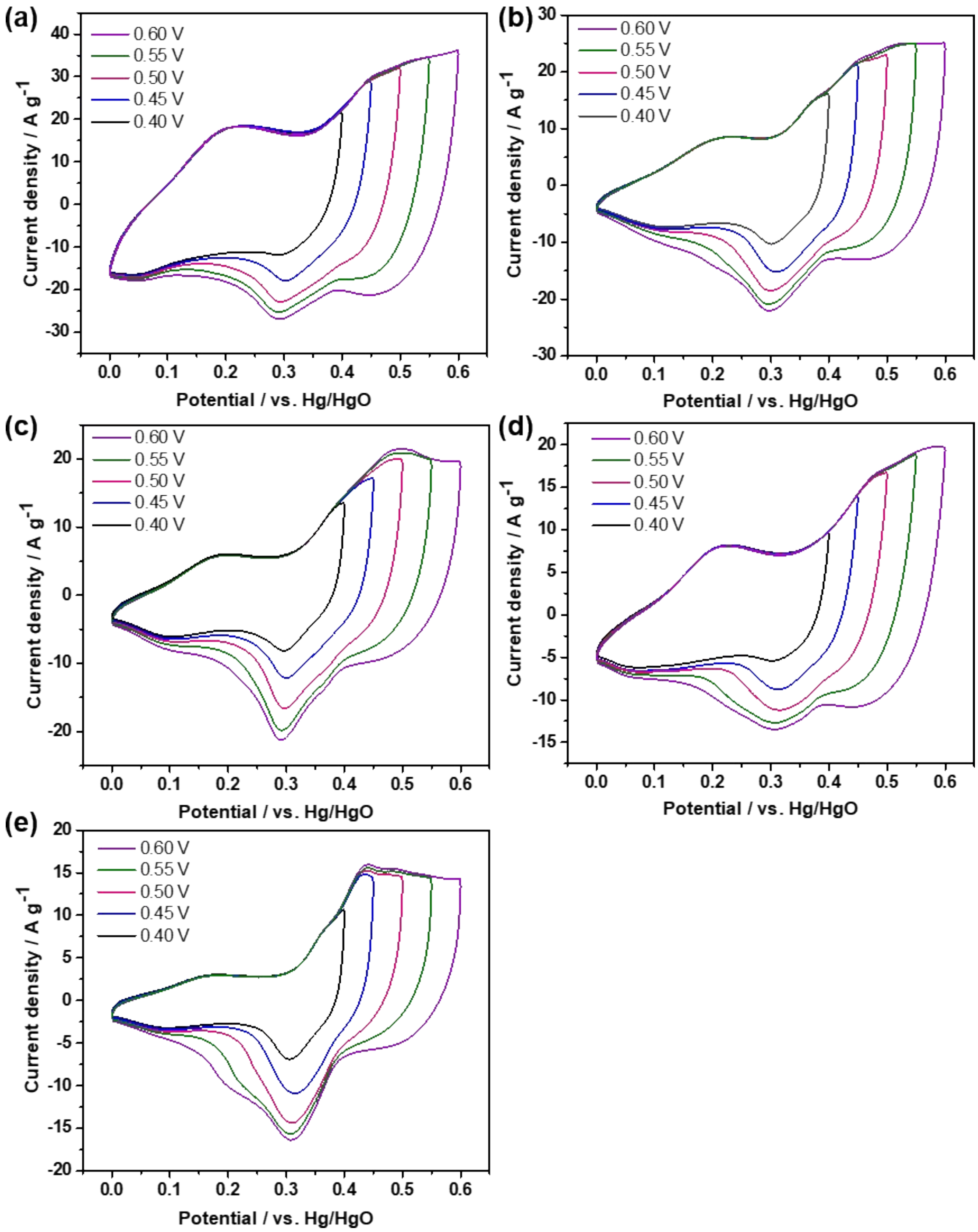

Fig. S17. CV curves of (a) α-$CoMn_{0.05}(OH)_x$/ZIF-67, (b) α-$CoNi_{0.05}(OH)_x$/ZIF-67, (c) α-$CoZn_{0.05}(OH)_x$/ZIF-67, (d) α-$Co(OH)_2$/ZIF-67 and (e) α-$Co(OH)_2$ at various voltage window.

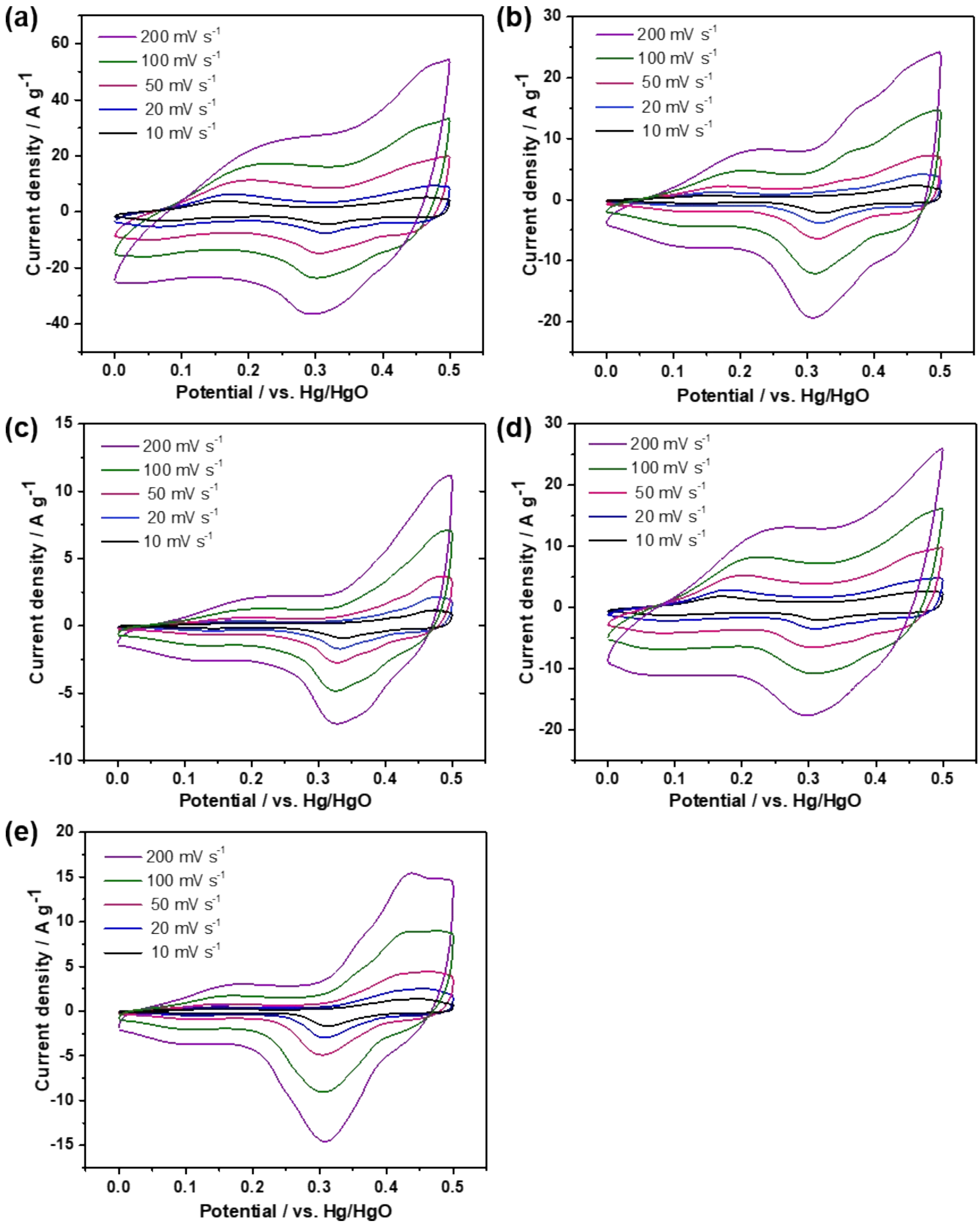

Fig. S18. CV curves of (a) α-CoMn$_{0.05}$(OH)$_x$/ZIF-67, (b) α-CoNi$_{0.05}$(OH)$_x$/ZIF-67, (c) α-CoZn$_{0.05}$(OH)$_x$/ZIF-67, (d) α-Co(OH)$_2$/ZIF-67 and (e) α-Co(OH)$_2$ at various scan rates.

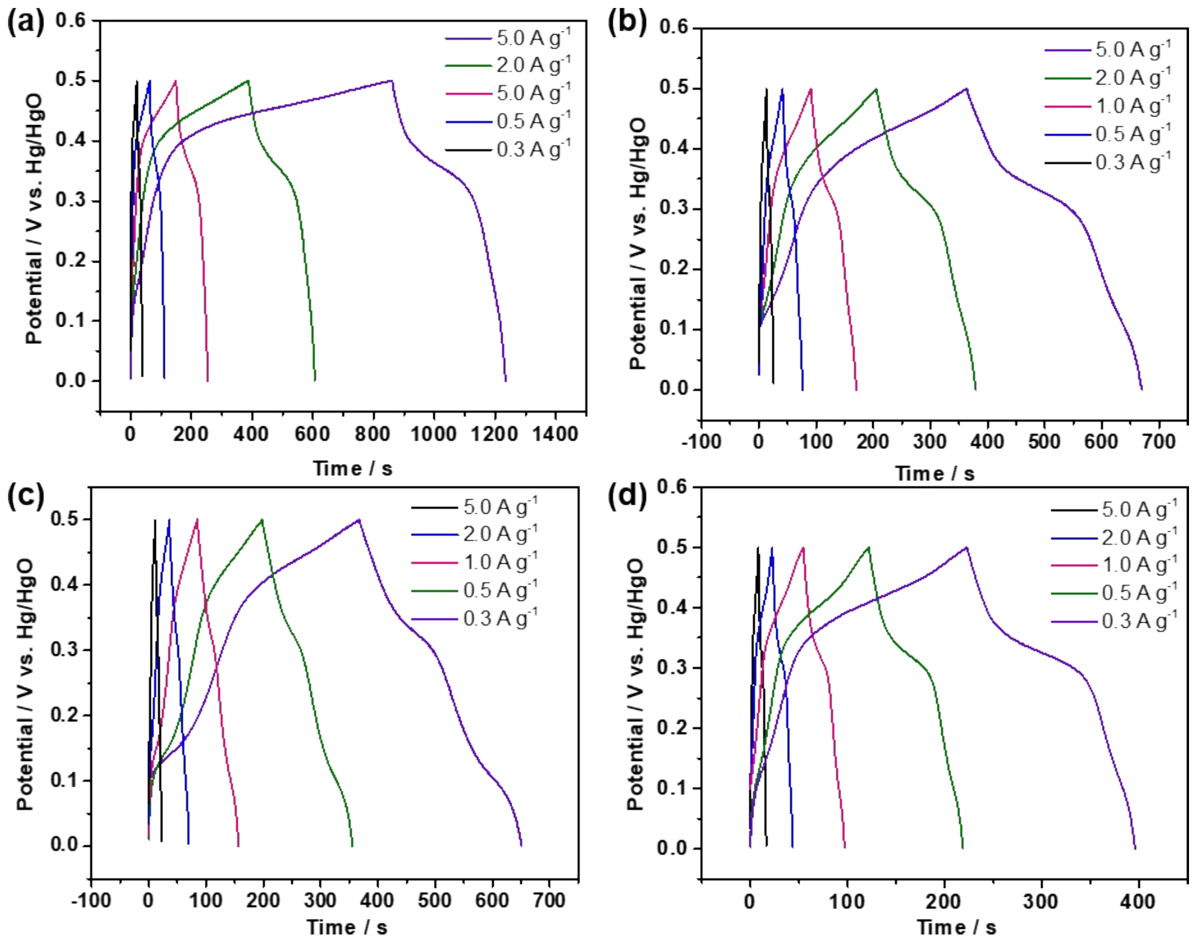

Fig. S19. GCD curves of (a) α-$CoNi_{0.05}(OH)_x$/ZIF-67, (b) α-$CoZn_{0.05}(OH)_x$/ZIF-67, (c) α-$Co(OH)_2$/ZIF-67 and (d) α-Co $(OH)_2$.

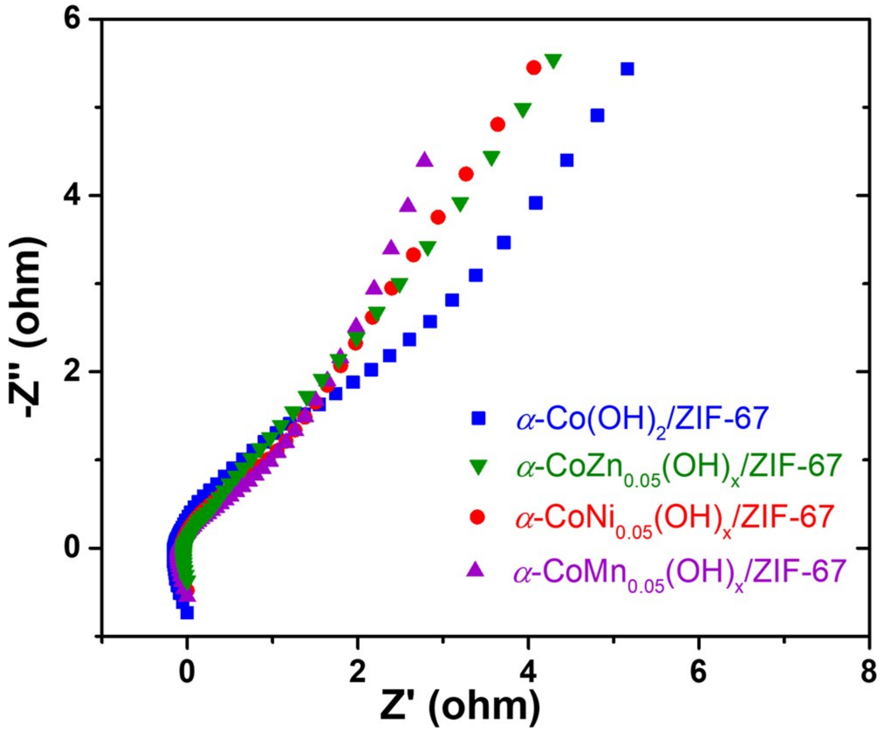

Fig. S20. Nyquist plots measured in the frequency range of 0.01-10^5 Hz.

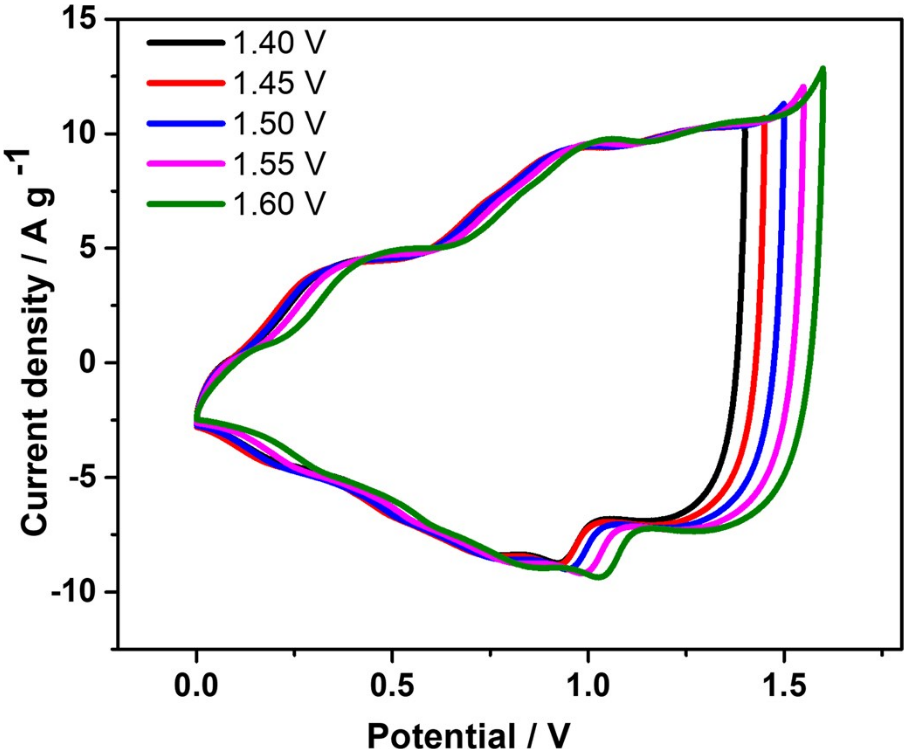

Fig. S21. CV curves of α-$CoMn_{0.05}(OH)_x$/ZIF-67//AC at various voltage windows.

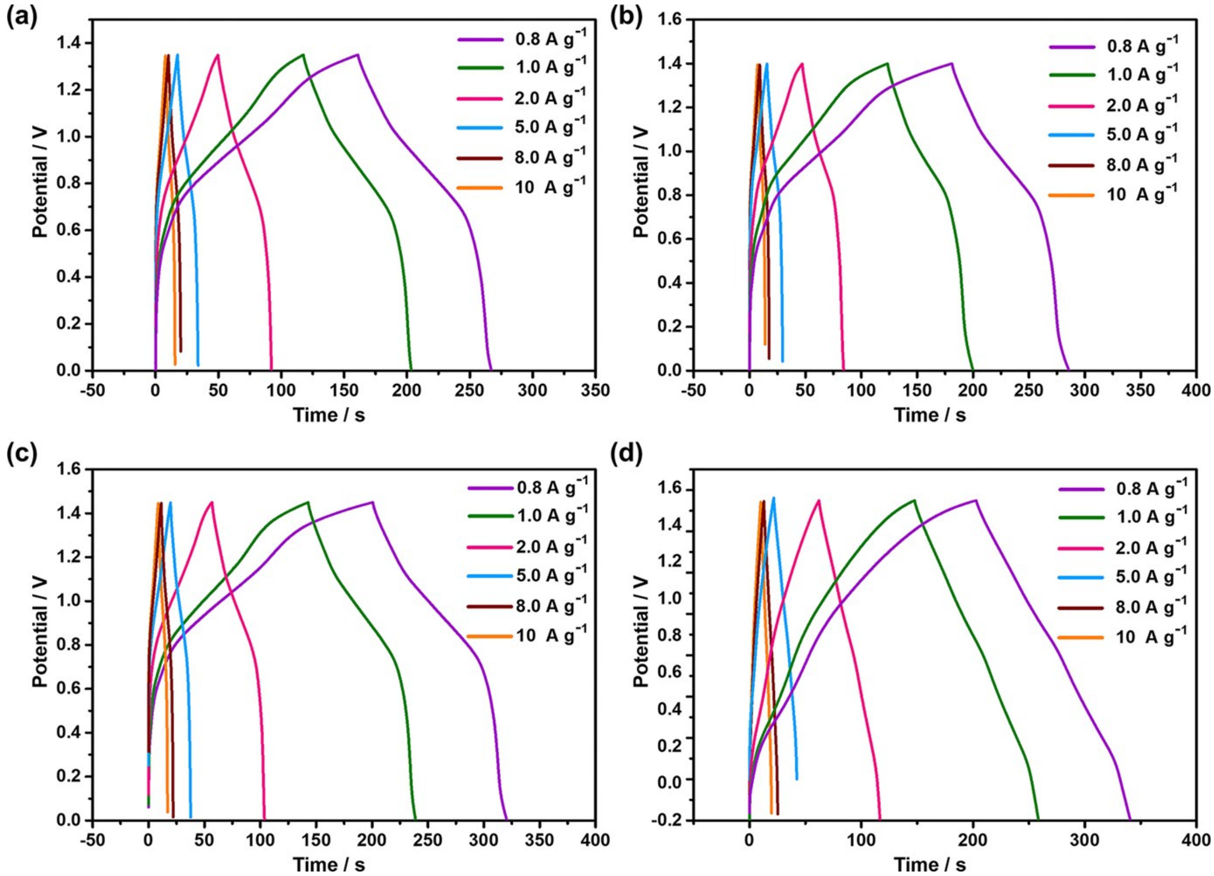

Fig. S22. GCD curves of α-$CoMn_{0.05}(OH)_x$/ZIF-67//AC at various voltage windows of (a) 0-1.35 V, (b) 0-1.40 V, (c) 0-1.45 V, and (d) 0-1.55 V.

Table S2. The relevant electrochemical properties of $Co(OH)_2$, LDH, ZIF-67 and their composites.

Material	Potential window / V	Electrolyte	Reference electrode	Specific capacitance / F g^{-1}	Cycling performance (Device)	Reference
CoOOH	-0.2-0.6	3 M KOH	Hg/HgO	198 F g^{-1} at 0.1 A g^{-1}	83% retention at 1 A g^{-1} after 5000 cycles	S1
α-$Co(OH)_2$	0-0.6	6 M KOH	Hg/HgO	345 F g^{-1} at 0.1 A g^{-1}	86% retention at 5 A g^{-1} after 15000 cycles	S2
α-$Co(OH)_2$	-0.1-0.6	6 M KOH	SCE	436 F g^{-1} at 50 mA cm^{-2}	549 F g^{-1} to 960 F g^{-1} (current density from 25 to 5 mA cm^{-2}) after 3000 cycles	S3
$(NiCo)(OH)_2/Cu(OH)_2$/CF	0-0.4	2 M KOH	SCE	849.6 C g^{-1} at 5 mA cm^{-2}	81.03% retention at 100 mA cm^{-2} after 5000 cycles	S4
$(NiCo)(OH)_2/NiCo_2O_4$	-0.1-0.45	2 M KOH	SCE	1132 F g^{-1} at 2 mA cm^{-2}	90% retention at 20 mA cm^{-2} after 2000 cycles	S5
Co(OH)2/CoNi-MOF	0.05-0.45	1 M KOH	SCE	1044 F g^{-1} at 2 A g^{-1}	94% retention after 5000 cycles	S6
ZIF-67	-0.3-0.25	6 M KOH	Ag/AgCl (3.5 M KCl)	103.6 F g^{-1} at 1 A g^{-1}	59% retention after 1000 cycles at 10 Ag^{-1} (TES)	S7
Mn doped ZIF-67	0-0.4	3M KOH	Hg/HgO	322 F g^{-1} at 3 A g^{-1}	64.1% retention after 1500 cycles at 10 Ag^{-1} (TES)	S8
rGO/ZIF-67	-0.3-0.25	6 M KOH	Ag/AgCl (3.5 M KCl)	210 F g^{-1} at 1 A g^{-1}	-	S7
ZIF-67/GO	-0.3-0.5	6 M KOH	SCE	202 F g^{-1} at 1 A g^{-1}	-	S9
Ni_{33}/ZIF-67/rGO_{20}	-0.2-0.8	1 M H_2SO_4	SCE	304.2 F g^{-1} at 1 A g^{-1}	87% retention after 4500 cycles	S10
NiAl LDH/Ni-MOF	0-0.5	6 M KOH	Hg/HgO	1086 F g^{-1} at 3 A g^{-1}	96.4% retention after 10000 cycles at 10 Ag^{-1}	S11
NiV LDH@ZIF-67	0-0.4	6 M KOH	-	830.6 F g^{-1} at 1 A g^{-1}	120% retention at 10 A g^{-1} after 5000 cycles	S12
$Ni_2CO_3(OH)_2$@ZIF-67	-0.15-0.4	6 M KOH	Ag/AgCl	697 F g^{-1} at 30 mV s^{-1}	-	S13

rGO@ZIF-67@NiAl-LDHs	0-0.36	6 M KOH	-	2291.6 F g^{-1} at 1 A g^{-1}	92% retention at 10 A g^{-1} after 4000 cycles	S14
ZIF-67@rGO	0-0.36	6 M KOH	-	90.5 F g^{-1} at 1 A g^{-1}	-	S14
rGO@NiAl-LDHs	0-0.36	6 M KOH	-	573.1 F g^{-1} at 1 A g^{-1}	-	S14
α-$CoMn_{0.05}(OH)_x$/ZIF-67	**0-0.5**	**3 M KOH**	**Hg/HgO**	**703.8 F g^{-1} at 0.3 A g^{-1}**	**96.2% retention at 500 mA cm^{-2} after 3500 cycles**	**This work**

Abbreviation: Saturated calomel electrode: SCE, Ultra-stable Y zeolite: USY, Copper foam: CF.

References

S1 C. Justin Raj, B. C. Kim, W. J. Cho, S. Park, H. T. Jeong, K. Yoo and K. H. Yu, *J. Electroanal. Chem.*, 2015, **747**, 130–135.

S2 F. Zhou, Q. Liu, J. Gu, W. Zhang and D. Zhang, *Electrochim. Acta*, 2015, **170**, 328–336.

S3 Z. Gao, W. Yang, Y. Yan, J. Wang, J. Ma, X. Zhang, B. Xing and L. Liu, *Eur. J. Inorg. Chem.*, 2013, **2013**, 4832–4838.

S4 D. Zhang, Y. Shao, X. Kong, M. Jiang, D. Lei and X. Lei, *Electrochim. Acta*, 2016, **218**, 294–302.

S5 X. Gong, J. P. Cheng, F. Liu, L. Zhang and X. Zhang, *J. Power Sources*, 2014, **267**, 610–616.

S6 T. Deng, Y. Lu, W. Zhang, M. Sui, X. Shi, D. Wang and W. Zheng, *Adv. Energy Mater.*, 2018, **8**, 1702294.

S7 A. Hosseinian, A. H. Amjad, R. Hosseinzadeh-Khanmiri, E. Ghorbani-Kalhor, M. Babazadeh and E. Vessally, *J. Mater. Sci. : Mater. Electron.*, 2017, **28**, 18040–18048.

S8 Y. Wenping, S. Xinyue, L. Yan and H. Pang, *J. Energy Storage*, 2019, **26**, 101018.

S9 W. Zhang, Y. Tan, Y. Gao, J. Wu, J. Hu, A. Stein and B. Tang, *J. Appl. Electrochem.*, 2016, **46**, 441–450.

S10 S. Sundriyal, V. Shrivastav, S. Mishra and A. Deep, *Int. J. Hydrogen Energy*, 2020, **45**, 30859–30869.

S11 W. Zheng, S. Sun, Y. Xu, R. Yu and H. Li, *ChemElectroChem*, 2019, **6**, 3375–3382.

S12 G. Wang, Y. Li, L. Xu, Z. Jin and Y. Wang, *Renew. Energy*, 2020, **162**, 535–549.

S13 Y. Gao, J. Wu, W. Zhang, Y. Tan, J. Gao, B. Tang and J. Zhao, *J. Appl. Electrochem.*, 2015, **45**, 541–547.

S14 D. Guo, X. Song, L. Tan, H. Ma, W. Sun, H. Pang, L. Zhang and X. Wang, *Chem. Eng. J.*, 2019, **356**, 955–963.